Calorimetric investigation of the formation of metastable silicides in Au/*a*-Si thin film multilayers

R. R. Chromik, L. Zavalij, M. D. Johnson, and E. J. Cotts
Department of Physics, Binghamton University, State University of New York, Binghamton, New York 13902-6016

(Received 22 September 2001; accepted for publication 12 November 2001)

Metastable phase formations were studied in Au/*a*-Si thin film multilayers using differential scanning calorimetry and x-ray diffraction. Two nonequilibrium crystalline silicides were found to form below 500 K. Each phase formed by a different mechanism, and the competing growth of the two phases over the temperature range of 375 to 500 K, was found to depend greatly on thickness and grain size in the Au layers. At higher temperatures (500–600 K), these metastable phases decomposed and the *a*-Si crystallized by metal-induced crystallization to yield a phase mixture of Au and *x*-Si. The enthalpy of crystallization of *a*-Si was measured from the calorimetry data to be -12.1 ± 1.2 kJ/mol. © *2002 American Institute of Physics.* [DOI: 10.1063/1.1432774]

I. INTRODUCTION

With length scales in electronic devices shrinking to the nanometer regime, a better understanding of the effect of grain boundaries and material interfaces on thermal and atomic processes is necessary. Thin films typically have high densities of grain boundaries and dislocations, providing paths for fast, short-circuiting atomic diffusion. These alternative reaction mechanisms have long been understood to greatly affect kinetics and phase selection in binary diffusion couples and thin film multilayers.[1–3] The work presented here on Au/*a*-Si multilayer thin films has provided an interesting example of the effects of reduced dimensions on the kinetics and energetics of thermal processes in a binary system.

The Au–Si system is a simple eutectic with no intermediate phase formations. However, many researchers have observed the formation of nonequilibrium phases, such as amorphous alloys and metastable crystalline alloys[4–21] that, in some cases, form by unique reaction kinetics (e.g., Harrison's type C).[4,22,23] The extensive work in the literature on characterizing metastable Au silicides was summarized most recently by Okamoto and Massalski.[8] Amorphous Au–Si alloys have been produced over a wide range of compositions (from 10 at. % Si to 90 at. % Si) by rapid quenching from the melt, laser irradiation, ion beam mixing, or sputter deposition. Many metastable crystalline phases have been observed, with stoichiometries varying from 11 to 33 at. % Si and different crystal structures. The work of Hultman *et al.*[7] reviewed the crystallography literature and proposed that the majority of diffraction data is consistent with a body centered cubic structure ($a=0.552$ nm) with nominal stoichiometry of Au_4Si. Although this observation is helpful in possibly connecting the different crystalline structures, no symmetry or atomic positions were identified by Hultman *et al.* for this sublattice or the cubic superstructure ($a=2.208$ nm) they observed experimentally. Two of the structures in the literature that have been observed by more than one group experimentally are a gamma brass structure ($a=0.96$ nm), first identified by Krutenat *et al.*[18] and Predecki, *et al.*,[20] and a second gamma brass structure with a larger lattice constant ($a=1.95$ nm) observed first by Luo *et al.*[21] These structures are labeled herein as γ_1 ($a=0.96$ nm), and γ_2 ($a=1.95$ nm), respectively. No obvious trends were identified from the literature as to which silicide phase will form (γ_1, γ_2, or some other silicide), even when a given sample preparation technique is used.

The diffusion mechanism by which a phase forms is often key to understanding the phase competition and resulting phase formation sequence in a binary system. In the literature for thin film Au–Si structures, there is evidence for the formation of crystalline Au silicides by annealing of amorphous Au–Si thin films[12,14,24] and by the metal-induced crystallization (MIC) of *a*-Si in Au/*a*-Si multilayers.[5,7,25–27] In the work of Koch *et al.*,[24] the formation of at least two metastable Au silicides was observed by annealing glassy Au–Si alloys prepared by sputtering and laser annealing. They were not able to unambiguously identify the two phases, but noted that the diffraction data from first phase was consistent with the γ_1 structure and an orthorhombic phase reported by Anderssen *et al.*[28] The second phase was reported by Koch *et al.* to be either the γ_2 phase or a hexagonal phase identified by M. von Allmen *et al.*[14]

Past studies of annealing of Au/*a*-Si multilayers offer the most intriguing results. The work of Hultman *et al.*[7] investigated the MIC of *a*-Si in a Au/*a*-Si single bilayer. As many researchers have observed,[5,7,25–27] the crystallization of *a*-Si takes place at drastically reduced temperatures in the presence of Au and other metals (450 K as opposed to 1000 K for pure *a*-Si). During this process, Hultman *et al.* observed the formation of a metastable Au silicide at temperatures of 450 K and above, with a lattice constant of 2.208 nm. The mechanism of Au diffusion into *a*-Si was concluded to be responsible for both the formation of the silicide and the MIC. In contrast, Seibt *et al.*,[4] who annealed Au/*a*-Si multilayers, defined the mechanism for the formation of a silicide in their samples as being grain boundary diffusion of Si into the Au layer followed by lateral growth (2D) of a Au

silicide at temperatures as low as 370 K. They identify this phase as the same Au silicide grown in the Hultman *et al.* work ($a = 2.208$ nm). Although most of Seibt's x-ray data indexes well with the pattern described by Hultman *et al.*, many of the peak positions in the pattern can only be indexed to other silicide phases.[29] The work of these two researchers[4,7] indicates the formation of metastable Au–Si alloys in similar Au/*a*-Si samples, but the mechanism identified for the growth of the alloy is entirely different.

In this study, the growth mechanisms for silicides in Au/*a*-Si thin films were examined to determine if microstructural differences are responsible for providing competing reaction mechanisms. Au/*a*-Si thin film multilayers with a wide range of layer thicknesses were used to examine the role of decreasing length scales and varying microstructure on the solid state reaction to form Au silicides at similar temperatures (300–550 K) to the two studies detailed above.[4,7] Differential scanning calorimetry (DSC) was used for the measurement of the heat flow associated with these thermal processes as the samples were heated from 300 K to temperatures between 600 and 660 K. Sample characterization and identification of reaction products was carried out using x-ray diffraction. Combining these two techniques, we have identified the formation of two metastable silicides (γ_1 and γ_2) in our samples that form by competing mechanisms that are highly dependent on the initial grain size of the Au. Finally, a determination of the crystallization enthalpy of *a*-Si was obtained by integration of the exothermic heat flow signals in numerous DSC experiments.

II. EXPERIMENT

Thin film multilayers of Au and *a*-Si were prepared in a sputter deposition chamber with a typical base pressure of 1×10^{-7} Torr. When preparing a multilayer, the chamber pressure was set to between 7 and 8 mTorr (high purity Ar gas), with some samples prepared at a pressure of 3 mTorr. Sputtering of Au was conducted with a dc magnetron sputtering gun, and an rf powered magnetron sputtering gun was used to sputter Si. Typical deposition rates were 0.15 nm/s for Au and 0.10 nm/s for Si.

Multilayers of Au and *a*-Si were created by timed, sequential sputter deposition of the two materials. In this manner, both a sample's average stoichiometry and modulation (sum of the thicknesses of one layer each of Au and *a*-Si), λ, could be controlled by changing the delay times for the substrate over each sputter gun. The average stoichiometry of the multilayer was selected to be between $Au_{53}Si_{47}$ and $Au_{49}Si_{51}$. The modulation for the samples varied between 6.1 and 64 nm.

After sputter deposition, samples were removed from the vented sample chamber and readied for x-ray diffraction analysis and differential scanning calorimetry experiments. The substrate, an NaCl crystal, was dipped in de-ionized water to obtain a freestanding Au/*a*-Si thin film. This thin film was rinsed in de-ionized water followed by rinsing with semiconductor grade acetone. The sample was then placed in a dry nitrogen atmosphere at 308 K for one hour. Lastly, the thin film was cut up using a razor blade. The smaller pieces would then be used for x-ray diffraction analysis or hermetically sealed for DSC experimentation.

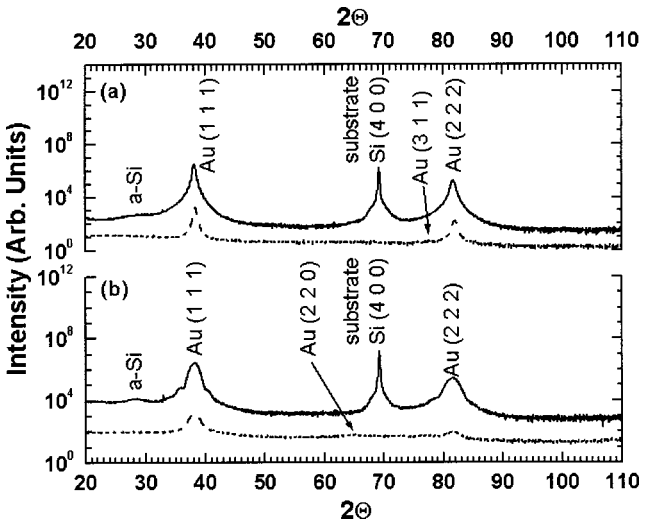

FIG. 1. X-ray diffraction data for as-prepared Au/*a*-Si multilayers of two different modulations, $\lambda = 47$ nm (a) and $\lambda = 14$ nm (b). Dashed curves are for samples prepared on NaCl substrates and solid curves are for samples prepared on Si(100). The samples exhibited a (111) preferred orientation for the peaks for Au and the typical broad peak for amorphous Si at approximately 28.5°.

In some cases, the substrate was a (100) oriented Si wafer. For these samples, x-ray diffraction experiments were carried out on the as-prepared film with the wafer being subsequently scored and broken into six or more smaller pieces to be annealed under an Ar atmosphere in a tube furnace. The annealed samples were examined with x-ray diffraction to further assist in phase identification in these thin films.

III. RESULTS AND DISCUSSION

A. X-ray diffraction study of Au/*a*-Si phase formations

As-prepared samples were characterized by x-ray diffraction, and, for Au/*a*-Si multilayers with $\lambda \geqslant 14$ nm, were determined to be phase mixtures of Au and *a*-Si. Figure 1 shows x-ray diffraction scans for samples of two different modulations: 47 nm, $Au_{0.53}Si_{0.47}$ [Fig. 1(a)], and 14 nm, $Au_{0.53}Si_{0.47}$ [Fig. 1(b)]. Also, for each sample modulation, Fig. 1 displays x-ray diffraction data for two different substrates: Si (solid curve) and NaCl (dashed curve). For these larger modulation samples, two strong peaks for Au are observed, i.e., Miller indices (111) and (222), and some intensity for the (220) and (311) peaks, indicating a (111) texture for Au in these samples of $\lambda \geqslant 14$ nm. It is also clear from the Au peaks in these x-ray diffraction scans that the grain size of the Au decreases with sample modulation. Using the (111) reflection as an example, the full width, half maximum (FWHM) value of this peak for the $\lambda = 47$ nm sample was 0.3°, but, for the $\lambda = 14$ nm sample, the FWHM was 1.5°. Using the method of integral breadths[30] to separate the contributions of the stress and the crystallite size on broadening of the peaks, the grain size of the Au for different modulations was calculated. It was found that the grain size scaled roughly with the individual Au layer thickness, meaning that the grain size was 6 nm for 14 nm modulation sample (7.5-

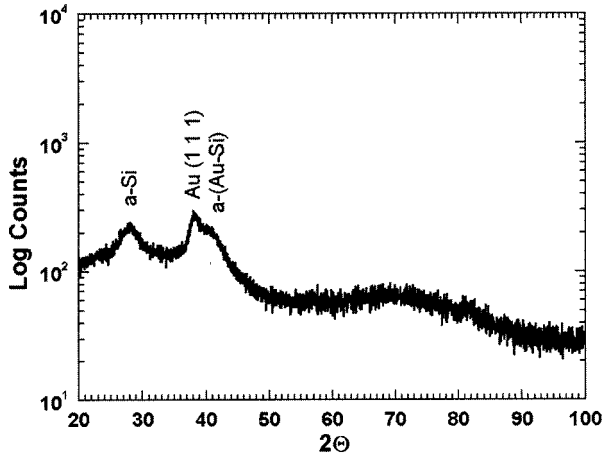

FIG. 2. X-ray diffraction data for a Au/*a*-Si sample prepared with a modulation of 6.1 nm. These data indicated the formation of an amorphous Au–Si alloy.

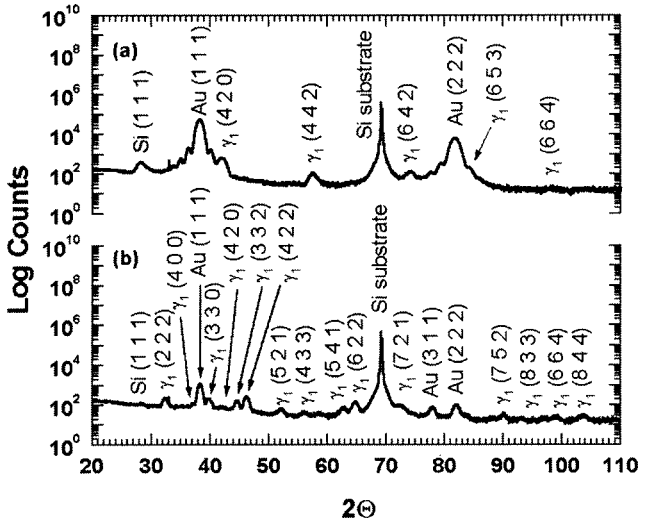

FIG. 3. X-ray diffraction data for Au/*a*-Si multilayers ($\lambda = 14$ nm) prepared on Si (100) and annealed at 423 K (a) and 513 K (b). Evidence is found for the growth of the γ_1 phase identified by Krutenat *et al.* (Ref. 18) at both temperatures.

nm-thick Au layers), and 22 nm for a 47 nm modulation sample (24.5-nm-thick Au layers). This result is in agreement with what was observed by previous investigators studying Au/*a*-Si multilayers fabricated by electron beam evaporation.[4,5,29]

Also present in the x-ray profiles of Fig. 1 is a broad peak centered at ≈28.5°, corresponding to *a*-Si. This peak is evident only in samples deposited on Si. For samples deposited on NaCl, a glass substrate supported the film during x-ray diffraction scans, and contributed a broad peak to the profiles that prevents the resolution of the peak for *a*-Si. When the *a*-Si peak was resolved, a Lorentzian curve was fit to the data and the FWHM value for this amorphous peak was determined to be approximately 5.5°. In terms of the scattering vector, $4\pi \sin\theta/\lambda$, this FWHM is 3.9×10^{-2} nm^{-1}. In a previous study on *a*-Si,[31] this peak was observed to occur at the same scattering vector for which we observe our peak, but with a slightly larger FWHM of 4.5×10^{-2} nm^{-1}.

For Au/*a*-Si multilayers with $\lambda < 7$ nm, x-ray diffraction data indicates the formation of significant amount of an amorphous Au–Si alloy. Figure 2 contains x-ray diffraction data for a sample prepared as an Au/*a*-Si composite with $\lambda = 6.1$ nm and $Au_{0.5}Si_{0.5}$. Two broad peaks are evident in this scan, the first at 28.2° with a FWHM of 5.2°, and the second at 41.0° with a FWHM of 4.3°. There is also a peak for the Au(111) reflection with a FWHM of 2.7°. The peak at 28.2° is associated with *a*-Si. The second broad peak indicates the formation of an amorphous Au–Si compound. The literature indicates that amorphous Au–Si alloys can be prepared over a wide composition range from 9 to 91 at. % Si.[8]

Phase formation in Au/*a*-Si films that had been prepared on Si(100) wafers was studied by performing furnace anneals at pertinent temperatures for between 5 and 15 min followed by quenching to room temperature. The annealed sections were then examined by x-ray diffraction. New Bragg peaks were observed for these annealed samples, indicating formations of metastable Au–Si compounds. X-ray diffraction scans for annealed small modulation samples ($\lambda = 14$ nm) are presented in Fig. 3. The first scan [Fig. 3(a)], for a sample annealed at 423 K, exhibits new Bragg peaks that are indexed to the γ_1 phase observed by Krutenat *et al.*[18] There is also evidence in this scan for the crystallization of *a*-Si. The peak for Si in this scan has a FWHM of 1.4°, indicating that some of the Si in the sample has transformed from the amorphous state to a small grained crystalline state. Annealing the sample at 513 K [Fig. 3(b)] resulted in additional Bragg peaks for the γ_1 phase, evidence for the formation of more of this metastable silicide. Also, the peak for Si in Fig. 3(b), although low in intensity, is still present and now exhibits a FWHM of 0.4°, suggesting further crystallization and grain growth has taken place. It has been previously observed that the reaction process in Au/*a*-Si multilayers finishes with Au diffusing to the outer surfaces of the multilayer stack.[7] The intensity of the Si peaks observed in all of our x-ray diffraction experiments is rather low, and can be attributed to the Si being buried in the bulk of the sample.

X-ray diffraction results for furnace annealed, larger modulation samples ($\lambda = 47$ nm) are shown in Fig. 4. For the sample annealed at 423 K [Fig. 4(a)], there is some indication of the growth of the γ_1 phase. Also, the broad peak for *a*-Si has disappeared, and has been replaced by a very low intensity peak corresponding to crystalline Si with a FWHM of 0.2°. At higher temperature (523 K), the phase formations are clearer, as shown in Fig. 4(b). For this sample with larger modulation, the indication is the growth of a phase identified by Luo *et al.*[21] This second phase, γ_2, has a large stoichiometric range of stability (0.25–0.50 at. % Si) and was best fit to a face centered cubic structure with $a = 1.905$ nm.

B. Calorimetry

Annealing of the Au/*a*-Si composites resulted in complex sequences of phase transformations that depended on the as-prepared state of the sample, especially on the Au thickness. This is depicted in Fig. 5, where the heat flow data

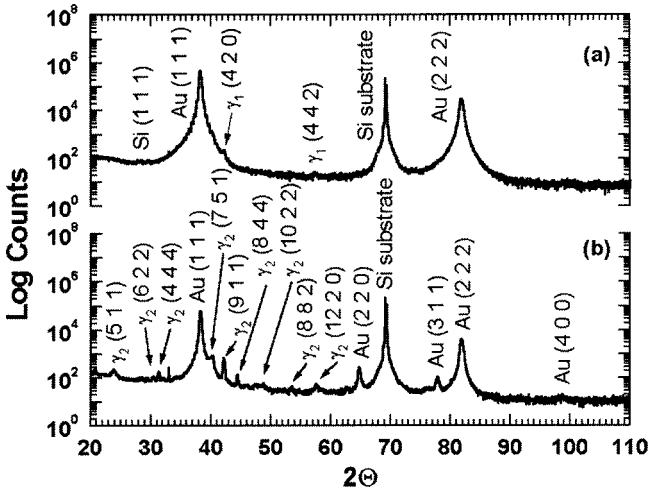

FIG. 4. X-ray diffraction data for Au/*a*-Si multilayers ($\lambda = 47$ nm) annealed at 423 K (a) and 523 K (b). Evidence is found for the formation of the γ_1 phase for the lower temperature anneal, and the formation of a second metastable silicide, identified as the γ_2 phase (Ref. 21), at higher temperatures.

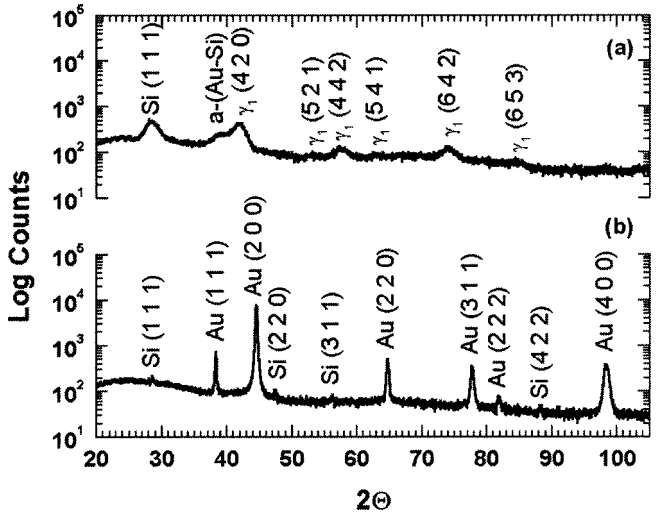

FIG. 6. X-ray diffraction data for Au/*a*-Si samples prepared with a modulation of $\lambda = 6.1$ nm that were heated to intermediate temperatures [462 K (a) and 648 K (b)] in a differential scanning calorimeter and then quenched to room temperature.

versus temperature (scan rate of 20 K/min) is presented for Au/*a*-Si samples with three different modulations. From the differences in heat flow data of these three traces, it is evident that each sample is somewhat unique in the manner by which it reacts upon heat treatment. Considering first the smallest modulation sample, $\lambda = 6.1$ nm [Fig. 5(a)], two transitions are identified: a crystallization process (labeled #1) and a final transition to equilibrium (labeled #2). More detail about these two transitions was obtained by heating portions of this sample to pertinent temperatures, immediately cooling to room temperature and then performing x-ray diffraction experiments. These x-ray diffraction results are presented in Fig. 6 for samples heated to 462 and 648 K. At 462 K, in between the two reactions for this sample, there is evidence for the formation of the metastable Au–Si phase, γ_1 [cf. Fig. 6(a)]. Also, the peak for Si in this scan has a FWHM of 2.4°, indicating some crystallization of fine grained Si occurs during the crystallization of the *a*-(Au–Si). These results indicate that reaction #1, including the shallow exotherm between 350 and 400 K, consists of the formation of the metastable, crystalline γ_1 phase at the expense of the *a*-(Au–Si) phase and partial crystallization of *a*-Si. X-ray diffraction data obtained for a sample heated through reaction #2 [Fig. 6(b)] indicates that the sample has transformed to a phase mixture of crystalline Au and Si. From this data, the exothermic peak labeled #2 in Fig. 5(a) is attributed to the decomposition of the γ_1 phase and final crystallization of any remaining *a*-Si.

To characterize phase formations for samples with $\lambda = 14.4$ nm [Fig. 5(b)], Au/*a*-Si multilayers were heated at 20 K/min to 453 and 623 K and quenched immediately to room temperature. Each sample was then examined by x-ray diffraction. These results are shown in Fig. 7. At the intermediate temperature of 453 K [cf. Fig. 7(a)], which lies between

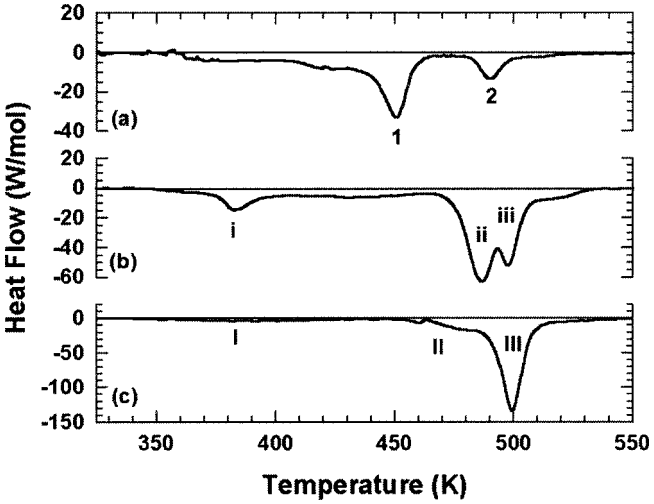

FIG. 5. Heat flow vs temperature measured by differential scanning calorimetry for Au/*a*-Si multilayers prepared with three different modulations: $\lambda = 6.1$ nm (a), $\lambda = 14$ nm (b) and $\lambda = 47$ nm (c).

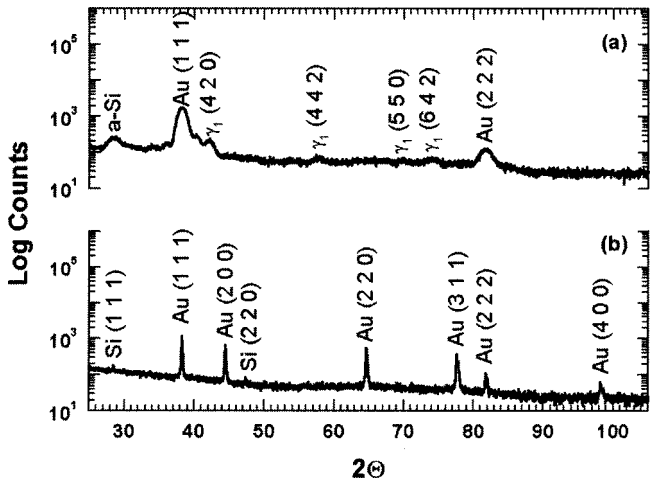

FIG. 7. X-ray diffraction data for samples with a modulation of $\lambda = 14$ nm that were heated to intermediate temperatures [453 K (a) and 623 K (b)] in a differential scanning calorimeter and then quenched to room temperature.

the first and second peak of the DSC trace for this sample [cf. Fig. 5(b)], there is evidence for the formation of the γ_1 phase identified by Krutenat *et al.*[18] In addition, there is a peak for the (1 1 1) reflection of Si with a FWHM value of roughly 2°. Thus, at the temperature of 453 K in the DSC trace shown in Fig. 5(b), both the formation of the metastable silicide phase, γ_1, and some relaxation or partial crystallization of the *a*-Si has occurred. For the samples heated to 623 K, peaks for Au and crystalline Si are observed. From this x-ray diffraction data, the exothermic peaks in Fig. 5(b) are associated with the formation of γ_1 from Au and *a*-Si (i), and the crystallization of *a*-Si and decomposition of the γ_1 phase (ii and iii).

For the sample of the largest modulation ($\lambda = 47$ nm) shown in Fig. 5(c), there is only one distinct exothermic peak in the heat flow (labeled III). Some other features exist in the scan: a very shallow exothermic signal between 350 and 450 K (labeled I), and an exothermic shoulder (labeled II) between 460 and 490 K that precedes the main exothermic peak at 500 K. To associate these peaks with thermal processes in the Au/*a*-Si multilayers, the x-ray diffraction data presented for furnace annealed samples [cf. Fig. 4] is examined again. For annealing at 423 K, evidence is found for the formation of the γ_1 phase. Annealing at 523 K resulted in the formation of the γ_2 phase. However, as with all our samples heated in the differential scanning calorimeter to above 550 K, the final state of the sample was found to be Au and Si. From the x-ray diffraction results for the $\lambda = 47$ nm sample, peak I is associated with the formation of small amounts of γ_1 phase, peak II is associated with the formation of the γ_2 phase, and the main exothermic peak (III) is associated with the decomposition of the metastable silicide and final crystallization of any remaining *a*-Si. The decomposition of the silicide and crystallization of *a*-Si are not resolved as separate peaks in the heat flow.

C. Thermodynamics of Au/*a*-Si reactions

Integration of exothermic peaks in the heat flow data of Fig. 5 yields enthalpy values that are attributed to distinct thermal processes, as identified by x-ray diffraction. For samples with the smallest modulations, $\lambda = 6.1$ nm [Fig. 5(a)], x-ray diffraction results indicate that the reaction taking place is:

$$a\text{-(Au–Si)} + x\text{-Au} + a\text{-Si} \rightarrow x\text{-Au} + x\text{-Si}, \quad \Delta H, \tag{1}$$

For samples with $\lambda \geqslant 14$ nm, x-ray diffraction results indicate that the overall reaction taking place is:

$$x\text{-Au} + a\text{-Si} \rightarrow x\text{-Au} + x\text{-Si}, \quad \Delta H. \tag{2}$$

Thus, integration of DSC scans for the larger modulation samples gives enthalpy values for Eq. 2, which represents the crystallization of *a*-Si. With a total of 26 scans performed for samples with $\lambda \geqslant 14$ nm, the crystallization enthalpy for *a*-Si was found to be -12.1 ± 1.2 kJ/mol. This value is consistent with a number of different values in the literature.[29,32–34] Table I lists the available data for the crystallization enthalpy of *a*-Si. In general, variations in these measurements can be attributed to the as-prepared state of the *a*-Si. It has long been speculated that *a*-Si can undergo a relaxation process attributed to small changes in bonding angles resulting in a more ordered, but still amorphous phase.[35] Thus, depending on the degree of relaxation in the as-prepared *a*-Si, one may expect differences in the total enthalpy measured for crystallization. Looking at Table I, the two studies that attempted to separate the relaxation enthalpy from the crystallization enthalpy found that this relaxation process can result in an enthalpy release as large as 3–5 kJ/mol.

TABLE I. The collected results from the literature for the crystallization enthalpy of *a*-Si, along with the measurement made here. The experimental technique for all investigations was differential scanning calorimetry.

Researcher	Sample (Preparation Technique)	Relaxation enthalpy (kJ/mol)	Crystallization enthalpy (kJ/mol)
This work	Au/*a*-Si (sputtered)	N/a	-12.1 ± 1.2
Gnauert[29]	Au/*a*-Si (electron beam)	N/a	-13.3 ± 0.6 -13.8 ± 0.8
Donovan *et al.*[32]	*a*-Si (ion implantation)	-5.1 ± 1.2	-13.4 ± 0.7
Roorda *et al.*[33]	*a*-Si (ion implantation)	-3.7 ± 0.2	-11.7 ± 1.0
Fan and Anderson[34]	*a*-Si (sputtered)	N/a	-10.0

Also of interest is the enthalpy associated with the formation of the metastable silicide phases. In our calorimetry results, the formation of the γ_1 phase is most clearly resolved for sample modulations of 14 nm. The peak labeled "*i*" in Fig. 5(b) is associated with the formation of the γ_1 phase. The reaction proceeding during peak *i*, is:

$$x\text{-Au} + a\text{-Si} \rightarrow \gamma_1, \quad \Delta H. \tag{3}$$

Using peak fitting software, the total heat released for the distinct peak at 380 K was calculated. The heat flow data in the region of 370–400 K was fit to a Lorentzian with the shallow heat release from 350 to 450 K being separated by including a baseline and two other peaks. For the ten samples for which the peak associated with Eq. 3 was resolved, the enthalpy was found to be -1.22 ± 0.23 kJ/mol, if it was assumed that all of the Au was consumed in forming the γ_1 phase. From x-ray data, it is clear that not all of the Au is consumed in the formation of γ_1. Thus, the value found here is a lower limit for the enthalpy ΔH for Eq. 3. Previous work on electron beam evaporated Au/*a*-Si samples found a value of -1.6 ± 0.3 kJ/mol for a reaction similar to Eq. 3, in which a metastable Au_3Si alloy was found to form instead of γ_1.[4,5,29]

In Fig. 8, the enthalpy of formation versus atomic percent Si is plotted for the Au–Si system. The point for *a*-Si is an average of the values in Table I, and the dashed line in the plot represents the enthalpy for a phase mixture of Au and *a*-Si. Also shown in Fig. 8 is the point for the enthalpy of a Au_3Si compound investigated by Gnauert,[29] and the enthalpy for the γ_1 phase as investigated by Chen and Turnbull.[19] Lastly, the lower limit for the driving force of Eq. 3 of -1.22 kJ/mol is also plotted in Fig. 8, indicated by an arrow and our datum (□).

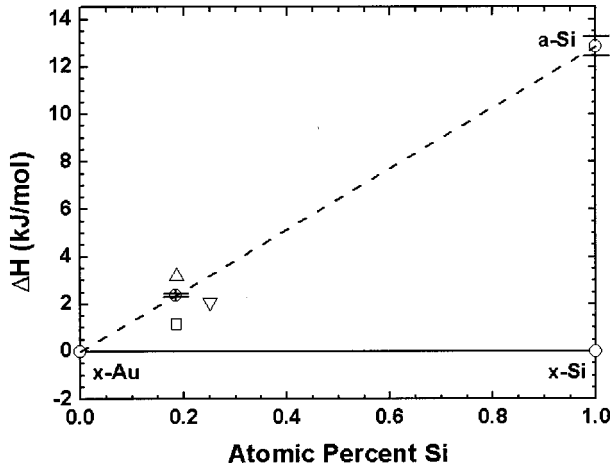

FIG. 8. A plot of the enthalpy of formation vs atomic percent Si for the Au–Si system. Data are plotted for the enthalpy of formation for pure elements and *a*-Si (O). The dashed line represents the enthalpy for a phase mixture of Au and *a*-Si. Three measurements are also plotted for the enthalpy of formation of metastable silicides: Chen and Turnbull (△) (Ref. 19), Gnauert (▽) (Ref. 29), and the measurement made here (□).

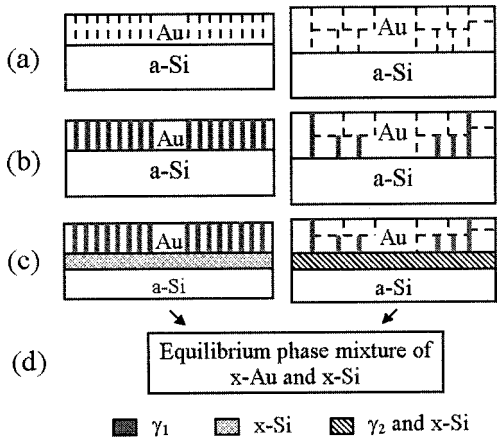

FIG. 9. A sketch of silicide formation processes in Au/*a*-Si thin films with modulations of $\lambda = 14$ nm and $\lambda \geqslant 47$ nm, based on the results of this work and silicide reaction mechanisms described in Refs. 4 and 7. The reaction sequence is as follows: (a) as-prepared samples have smaller grain size in the Au layer for smaller modulations, (b) heating the samples to ≈400 K results in the formation of the γ_1 phase by grain boundary diffusion of Si in the Au layer, (c) at ≈450 K, diffusion of Au into the *a*-Si results in the crystallization of *a*-Si, and for the larger modulation samples, the formation of the γ_2 phase, (d) heating above 550 K, the sample converts to a phase mixture of Au and *x*-Si.

Consideration of the magnitude of the enthalpy of formation of Au silicides of compositions near 80 at. % Au from crystalline Au and Si provides an indication of why these compounds form so readily by a variety of mechanisms. As illustrated in Fig. 8, our determination of the lower limit of the enthalpy of formation of γ_1 from *a*-Si and Au implies that the upper limit on the enthalpy of formation of γ_1 from crystalline Si and Au is +1.1 kJ/mol. As mentioned above, our measurement is consistent with that of Gnauert *et al.*[29] while the measurement of Chen and Turnbull,[19] who used bulk samples of γ_1, indicates a higher enthalpy of formation. The data presented in Fig. 8 indicates that the enthalpy of formation for Au silicides near the eutectic composition (18.6 at. % Si) is relatively small, approximately 1 kJ/mol in magnitude. Given the positive, albeit small, increase in entropy upon alloy formation, the free energy difference between γ_1 and a phase mixture of Au and Si is even smaller in magnitude. This measurement of the enthalpy of formation provides thermodynamic evidence that supports numerous observations that these metastable Au silicides are easily prepared by many techniques making use of nonequilibrium conditions.

D. Metastable silicide growth mechanisms and their competition

The differences in the heat flow signals for samples of different modulations merits a discussion of the mechanisms of silicide formation and *a*-Si crystallization in this system. The differences between the larger modulation samples ($\lambda \geqslant 14$ nm) and the small modulation sample ($\lambda = 6.1$ nm) is primarily due to the presence of the amorphous Au–Si compound in the latter. However, the differences between the heat flow data for the $\lambda = 14.4$ and 47 nm samples [Fig. 5(b) and Fig. 5(c), respectively] are due to more subtle differences in the samples. Two previous researchers have examined the Au–Si system in connection with the crystallization of *a*-Si, and each derived different mechanisms for silicide formation and the eventual crystallization of the *a*-Si. Hultman *et al.*[7] used a bilayer of Au/*a*-Si and found that at temperatures of 450 K and above, Au diffused into the *a*-Si layer, resulting in the nucleation of *x*-Si that was surrounded by a Au–Si compound. In contrast, Seibt *et al.*,[4] found that grain boundary diffusion of Si into the Au layer (Harrison type C kinetics[23]) resulted in the formation of a metastable silicide that then grew laterally (2D) within the Au layer at temperatures as low at 370 K. The results for our calorimetry data and phase identification work are consistent with both of these mechanisms. Figure 9 is a sketch of how these two mechanisms compete in our "thin" ($\lambda = 14$ nm) and "thick" ($\lambda = 47$ nm) film Au/*a*-Si multilayers. For the as-prepared state, x-ray diffraction data indicated a smaller grain size for the smaller modulation sample [Fig. 9(a)]. This results in more available grain boundaries for diffusion of Si into the Au layer and substantial formation of the γ_1 phase. In the sample with a thicker Au layer and larger grain size, fewer grain boundaries are present, and there is the possibility of unfavorable diffusion paths once the Si has entered the Au layer, resulting in the formation of only a small amount of γ_1. This explains the presence of a distinct exotherm for the formation of γ_1 in the $\lambda = 14$ nm samples and only a shallow exotherm for the $\lambda = 47$ nm samples. Now, with the samples heated to 450 K and above, the mechanism described by Hultman *et al.* becomes available. Au atoms diffuse into the *a*-Si layer, resulting in crystallization of *a*-Si and possibly more silicide formation. However, for the small modulation sample, much of the Au is used up by the formation of γ_1. What Au does diffuse into the *a*-Si layer is not enough to form the Au-rich γ_2 phase. In contrast, for the $\lambda \geqslant 47$ nm samples, much of the Au remains unreacted, allowing for both the crystallization of *a*-Si and the formation of the γ_2 phase within the *a*-Si layer. This explains the presence of the

secondary phase formation in the larger modulation samples. For both samples, heating above 550 K results in the decomposition of the metastable silicides and transformation of the sample to equilibrium components of Au and x-Si.

IV. CONCLUSIONS

Metastable silicide formations and metal-induced crystallization in Au/a-Si thin film multilayers were investigated. Two metastable silicides, γ_1 and γ_2, grew in the thin films by different reaction mechanisms. Varying the thickness of the Au layer resulted in variation in the grain size. The reaction mechanism for γ_1 silicide growth was found to depend on the availability of grain boundaries, while the growth of γ_2 apparently proceeded by Au diffusion into the a-Si layer. Heating of the multilayers to 600 K resulted in the decomposition of the metastable silicides and the transformation of the samples to equilibrium components of x-Au and x-Si. The net reaction over this temperature range was the crystallization of a-Si, with $\Delta H_c^{a\text{-Si}}$ determined to be -12.1 ± 1.2 kJ/mol.

ACKNOWLEDGMENTS

This work was supported in part by grants from the National Science Foundation (DMR-9902783 and DMR-9976713) and by the Integrated Electronics Engineering Center (IEEC) at the State University of New York at Binghamton. The IEEC is a New York State Center for Advanced Technology, and receives funding from the New York State Office of Science, Technology and Academic Research and a consortium of industrial members.

[1] R. R. Chromik, W. K. Neils, and E. J. Cotts, J. Appl. Phys. **86**, 4273 (1999).
[2] K. R. Coffey and K. Barmak, Mater. Res. Soc. Symp. Proc. **343**, 193 (1994).
[3] Z. G. Xiao, J. W. Honeycutt, and G. A. Rozgonyi in *Evolution of Thin-Film and Surface Microstructure*, edited by C. V. Thompson, J. Y. Tsao, and D. J. Srolovitz (Mater. Res. Soc. Proc., Pittsburgh, PA, 1991), Vol. 202, pp. 259–264.
[4] M. Seibt, S. Buschbaum, U. Gnauert, W. Schröter, and D. Oelgeschläger, Phys. Rev. Lett. **80**, 774 (1998).
[5] M. Seibt, S. Buschbaum, and U. Gnauert, Inst. Phys. Conf. Ser. **146**, 545 (1995).
[6] P.-H. Chang, G. Berman, and C. C. Shen, J. Appl. Phys. **63**, 1473 (1988).
[7] L. Hultman, A. Robertsson, H. T. G. Hentzell, I. Engrtröm, and P. A. Psaras, J. Appl. Phys. **62**, 3647 (1987).
[8] H. Okamoto and T. B. Massalski, Bull. Alloy Phase Diagrams **4**, 190 (1983).
[9] B. Y. Tsaur and J. W. Mayer, Philos. Mag. A **43**, 345 (1981).
[10] N. G. Dhere and C. A. Loural, Thin Solid Films **81**, 213 (1981).
[11] S. S. Lau, B. Y. Tsaur, M. von Allmen, J. W. Mayer, B. Stritzker, C. W. White, and B. Appleton, Nucl. Instrum. Methods **182/183**, 97 (1981).
[12] G. Marchal, P. Mangin, and C. Janot, Philos. Mag. B **42**, 81 (1980).
[13] H. L. Gaigher and N. G. Van der Berg, Thin Solid Films **68**, 373 (1980).
[14] M. von Allmen, S. S. Lau, M. Mäenpää, and B. Y. Tsaur, Appl. Phys. Lett. **36**, 205 (1980).
[15] R. P. Anantatmula, A. A. Johnson, S. P. Gupta, and R. J. Horylev, J. Electron. Mater. **4**, 445 (1975).
[16] C. Suryanarayana and T. R. Anantharaman, Mater. Sci. Eng. **13**, 73 (1974).
[17] E. Philofsky, K. V. Ravi, J. Brooks, and E. Hall, J. Electrochem. Soc. **119**, 527 (1972).
[18] R. C. Krutenat, J. K. Tein, and D. E. Fornwalt, Metall. Trans. **2**, 1479 (1971).
[19] H. S. Chen and D. Turnbull, J. Appl. Phys. **38**, 3646 (1967).
[20] P. Predecki, B. C. Geissen, and N. J. Grant, Trans. Metall. Soc. AIME **233**, 1438 (1965).
[21] H. L. Luo, W. Klement, Jr., and T. R. Anantharaman, Trans. Indian Inst. Met. **18**, 214 (1965).
[22] R. W. Balluffi and J. M. Blakely, Thin Solid Films **25**, 363 (1975).
[23] L. G. Harrison, Trans. Faraday Soc. **57**, 1191 (1961).
[24] N. Koch, U. Kambli, and M. von Allmen, J. Phys. D **21**, 1142 (1988).
[25] F. A. Quli and J. Singh, Mater. Sci. Eng., B **67**, 139 (1999).
[26] K. H. Lee, Y. K. Fang, and S. H. Fan, Electron. Lett. **35**, 1108 (1999).
[27] M. S. Ashitkar and G. L. Sharma, Jpn. J. Appl. Phys. **34**, 5520 (1995).
[28] G. A. Anderssen, J. L. Bestel, A. A. Johnson, and P. Post, Mater. Sci. Eng. **7**, 83 (1971).
[29] U. Gnauert, Dissertation zur Erlangung des Doktogrades, U. Göttingen, 1994.
[30] H. P. Klug, *X-ray Diffraction Procedures for Polycrystalline and Amorphous Materials* (Wiley, New York, 1974), pp. 661–665.
[31] S. C. Moss and J. F. Graczyk, Phys. Rev. Lett. **23**, 1167 (1969).
[32] E. P. Donovan, F. Spaepen, J. M. Poate, and D. C. Jacobson, Appl. Phys. Lett. **55**, 1516 (1989).
[33] S. Roorda, S. Doorn, W. C. Sinke, P. M. L. O. Scholte, and E. van Loenen, Phys. Rev. Lett. **62**, 1880 (1989).
[34] J. C. C. Fan and C. H. Anderson, Jr., J. Appl. Phys. **52**, 4003 (1981).
[35] W. C. Sinke, S. Roorda, and F. W. Saris, J. Mater. Res. **3**, 1201 (1988).